

Predicting Driver’s Perceived Risk: a Model Based on Semi-Supervised Learning Strategy

Siwei Huang, Chenhao Yang and Chuan Hu

Abstract— Drivers’ perception of risk determines their acceptance, trust, and use of the Automated Driving Systems (ADSs). However, perceived risk is subjective and difficult to evaluate using existing methods. To address this issue, a driver’s subjective perceived risk (DSPR) model is proposed, regarding perceived risk as a dynamically triggered mechanism with anisotropy and attenuation. 20 participants are recruited for a driver-in-the-loop experiment to report their real-time subjective risk ratings (SRRs) when experiencing various automatic driving scenarios. A convolutional neural network and bidirectional long short-term memory network with temporal pattern attention (CNN-Bi-LSTM-TPA) is embedded into a semi-supervised learning strategy to predict SRRs, aiming to reduce data noise caused by subjective randomness of participants. The results illustrate that DSPR achieves the highest prediction accuracy of 87.91% in predicting SRRs, compared to three state-of-the-art risk models. The semi-supervised strategy improves accuracy by 20.12%. Besides, CNN-Bi-LSTM-TPA network presents the highest accuracy among four different LSTM structures. This study offers an effective method for assessing driver’s perceived risk, providing support for the safety enhancement of ADS and driver’s trust improvement.

I. INTRODUCTION

With the development of automated vehicles (AVs), safety has been recognized as the key bottleneck limiting the progress and widespread adoption of autonomous driving [1]. Reports of safety problems and accidents continue to hinder public confidence and acceptance of AVs [2]. How to meet driver’s expectations for the safety of automated driving systems (ADSs) becomes a crucial issue [3]. Well-considered approaches to perceived risk assessment are needed.

Tradition research mostly focuses on objective risks in traffic scenarios. However, because of ADS’s imperfect performance and black-box behavior, driver’s perceived risk may not be consistent with the objective risk in traffic environments. Considering this, risk should be comprehensively assessed from both objective risk and driver’s perceived risk perspectives. The following sections will separately introduce these two perspectives.

A. Objective Risk Assessment and Modeling

Crash frequency and severity are important evaluation indicators for the safety of ADS [4]. However, collisions

are rare events. Thus, specific and quantifiable criteria are applied to evaluate objective risk. Common methods are rule-based methods and learning-based methods [5].

Rule-based methods assess risk using objective indicators from the traffic environment, with Surrogate Safety Measures (SSMs) and Risk Field (RF) being two common approaches. SSMs describe the conflicts between users in the traffic environment in terms of time and space, such as time to collision (TTC) and time headway (TWH). RF generally considers the kinematics of all traffic objects to build risk models. Wang et al. [6] developed a Driving Safety Field (DSF) model by overlaying potential fields, kinetic fields, and behavior fields. Chen et al. [7] proposed a Potential Damage Risk (PODAR) describing potential damage by energy and decay functions.

However, rule-based methods perform poorly in assessing coupled risks of complex traffic environment. Machine learning methods have a distinct advantage under this condition. Xie et al. [8] collected driver’s operation, visual, physiological, and vehicle kinematic data, predicting risk levels through an Att-Bi-LSTM network. Liu et al. [9] used a Transformer network to capture complex interaction dynamics between pedestrians and vehicles to predict their collision risks.

B. Driver’s Perceived Risk Assessment and Modeling

Drivers form judgements about the risk when they are in traffic environment. Limited attention and working memory hinder them from acquiring and interpreting all information [10]. That’s why driver’s subjective perceived risk often does not align with the objective risk in traffic environment.

Investigating driver’s perceived risk requires collecting feedback from the human driver, where driver-in-loop experiments are essential. Simulator experiments [11], real vehicle experiments [12], and video experiments [13] are conducted to provide driving scenarios. Interval rating [14] and continuous rating through equipment [13] are conducted to obtain driver’s real-time subjective risk ratings (SRRs). For example, Ping et al. [13] presented real-world driving videos to drivers while continuously collecting their SRRs via computer buttons. They extracted a semantic understanding of traffic scenes from visual images and used a GRU network to predict driver’s perceived risk. Yu et al. [14] collected SRRs ranging from -2 to 2 for lane-change segments through simulator experiment. They used a graph convolution network and LSTM network to predict driver’s perceived risk.

Objective indicators from traffic environment are complex and unpredictable. Some studies suggest preliminary model-

arXiv:2504.12665v1 [cs.LG] 17 Apr 2025

This work was supported by the Outstanding Youth Science Foundation Project (Overseas) of National Natural Science Foundation of China (NSFC) under grant number 24Z990200855.

*Chuan Hu is the corresponding author.

Siwei Huang, Chenhao Yang and Chuan Hu are with School of Mechanical Engineering, Shanghai Jiao Tong University, Shanghai, China sisi-twt-24@sjtu.edu.cn, chenhaoyan3039@sjtu.edu.cn, chuan.hu@sjtu.edu.cn

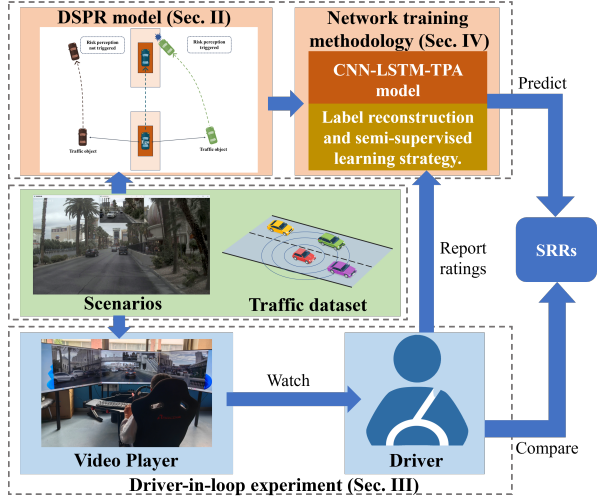


Fig. 1. Framework of our study.

ing of these indicators before integrating them with drivers' SRRs for further analysis. For example, based on RF model and spatiotemporal distribution of driver's cognitive risk, Song et al. [5] developed a machine learning-based method for predicting subjective risk in lane-changing scenarios.

To reduce noise and improve consistency of SRRs, some studies have also introduced semi-supervised learning [15]. Additionally, semi-supervised learning is effective in learning risk patterns from a small amount of labeled data combined with a large volume of unlabeled data [16]. However, few studies have applied it to driver's perceived risk assessment.

C. The Current Research

Although existing research has made significant progress in objective risk assessment, there is still limited research on driver's perceived risk. Furthermore, few studies have integrated objective and subjective risks for a comprehensive analysis. To address these issues, we propose a driver's perceived risk (DSPR) model and utilize machine learning methods to predict driver's SRRs. The main contributions of this paper are as follows: (1) Proposed DSPR model considers both objective risk and driver's risk perception patterns, with a risk-trigger mechanism introduced; (2) We introduce a semi-supervisor learning strategy with a convolutional neural network and bidirectional long short-term memory network with temporal pattern attention (CNN-Bi-LSTM-TPA) for driver's SRRs prediction.

The rest of this paper is organized as follows: Section II introduces the established DSPR model. Section III introduces the experiment and the data collection method. Section IV introduces the network training methodology. Section V presents results and discussion. Section VI concludes this work. The framework of our study is shown in Fig. 1.

II. THE MODELLING OF DRIVER'S PERCEIVED RISK

According to the situation awareness (SA) theory [10], driver's perception of the situation occurs at three levels: 1) Perception of the elements in the environment; 2) Comprehension of the current situation; 3) Projection of future status.

Most existing RF models describe the second level, while neglecting the other two. Considering this issue, we propose DSPR to considers both objective risk and driver's perception patterns. Incorporating the concept from [7], we define driver's perceived risk as "the expectation and assessment of the likelihood and severity of a risk event." We introduce the risk-trigger mechanism for the first level, observation sensitivity for the second level, and time and spatial decay of risk for the third level of SA theory. The basic formula of DSPR is shown in (1):

$$\mathbf{R}(t) = [\mu_1 R_1(t) \quad \dots \quad \mu_i R_i(t) \quad \dots \quad \mu_n R_n(t)] \quad (1)$$

where $\mathbf{R}(t)$ is the perceived risk sequence calculated from DSPR; $R_i(t)$ is the risk of traffic object O_i at current timestamp t ; μ_i is the sensitivity coefficient of O_i ; n is the total number of considered traffic objects.

A. Risk-trigger Mechanism

The concept of the risk-trigger mechanism stems from the idea that a driver's attention and perception are limited. As shown in Fig. 2, we assume that only traffic object O_i entering a dynamic risk perception domain (RPD) within the prediction time t_p from current moment will cause the driver to perceive risk (risk perception is triggered). It can prevented risk from extending indefinitely, focusing on the risks that related to the ego vehicle. We assume that the acceleration of the ego vehicle and traffic objects remain stable within t_p .

If the risk perception is triggered, R_i is defined in (2).

$$R_i(t) = \alpha_t \cdot \alpha_s \cdot s_\theta \cdot E_{p_i}^{tr} \quad (2)$$

where α_t is the time decay coefficient; α_s is the spatial decay coefficient; s_θ is the driver's observation sensitivity; $E_{p_i}^{tr}$ is the relative kinetic energy.

If the risk perception is not triggered, the driver will only perceive risk from the ego vehicle. R_i is defined in (3).

$$R_i(t) = s_\theta \cdot E_{e_i}^{tr} \quad (3)$$

where $E_{e_i}^{tr}$ is the relative kinetic energy of ego vehicle.

To simplify calculation, we consider the shape of vehicles and RPDs as a rectangle. The shape of the RPD is variable. The idea comes from THW. For longitudinal risk, driver's perception distance increase with ego vehicle's velocity, while almost doesn't change for lateral risk. We define the weak RPD (w-RPD) where driver perceives risk, and the strong RPD (s-RPD) where driver strongly perceives risk. We denote the length of ego vehicle as L , width as W , velocity as v_{ego} , the time headway threshold of the w-RPD and s-RPD as THW_w and THW_s . The length of the w-RPD is $l_w = 2(L + THW_w \cdot v_{ego})$; the width of the w-RPD is $w_w = 5W$; the length of s-RPD is $l_s = 2(L + THW_s \cdot v_{ego})$; the width of s-RPD is $w_s = 2W$.

B. Time Decay and Spatial Decay of Risk

1) *Time decay coefficient.* We denote the time from the current timestamp t to the time of risk activation as t_r . The earlier this moment occurs, the more clearly the driver

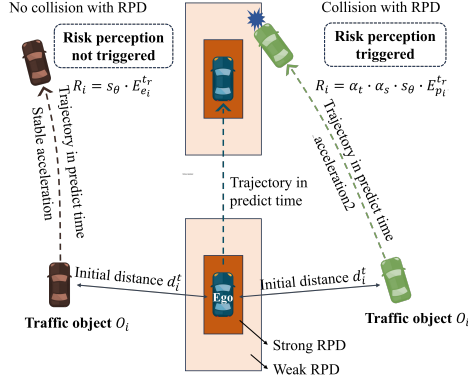


Fig. 2. The RPD and the risk perception triggering mechanism.

perceives the risk. When O_i enters RPD at t_r within t_p , the time decay coefficient α_t is defined in (4).

$$\alpha_t = \frac{t_p}{t_p + t_r} \quad (4)$$

2) *Spatial decay coefficient.* The spatial decay coefficient α_s reflects how the distance from a traffic object affects the driver's perception of risk. As shown in (5), α_{ss} is the coefficient of s-RPD, α_{ws} is the coefficient of w-RPD α_{ws} .

$$\alpha_s = \alpha_{ss} \cdot \alpha_{ws} \quad (5)$$

Drivers have different tolerances for safe distances in various directions. We use a sine function to model the differences in tolerance across directions. d_i^t is the initial distance between ego vehicle and O_i at t . The straight-ahead of ego vehicle is 0° , and rear is 180° . θ_i^t is the initial angle of O_i from from the ego vehicle's perspective, θ_{wi} is the angle of the collision position with the w-RPD (if collision happens). Within t_p , if O_i collides with the s-RPD, We define that $\alpha_{ss} = \frac{l_{\text{strong}} - \sin \theta_i^t \cdot (l_{\text{strong}} - w_{\text{strong}})}{d_i^t}$ and $\alpha_{ws} = 1$. If O_i collides with the w-RPD, α_{ss} keeps the same and $\alpha_{ws} = \frac{l_{\text{strong}} - \sin \theta_{wi} \cdot (l_{\text{strong}} - w_{\text{strong}})}{d_i^{t_r}}$.

C. Driver's observation sensitivity.

Driver's observation exhibits anisotropy. Their attention usually focuses on the road ahead, leading to neglect of other areas. The observation sensitivity s_θ can balance the weight of risk among surrounding traffic objects in (6). As shown in Fig. 3, for 0° to 30° , traffic objects are easily noticeable, so s_θ is at its maximum. For 30° to 75° , traffic objects are gradually not easy to notice. For 75° to 150° , the driver needs to turn their head to observe around, and s_θ gradually reaches its minimum value. For 150° to 180° , driver can observe through the rearview mirror, and s_θ is above the minimum value.

D. Relative Kinetic Energy.

We use a concept of kinetic energy to describe the driver's expectations regarding collision consequences. The relative kinetic energy $E_{p_i}^{t_r}$ is defined in (7). Where $v_{b_i}^{t_r} = v_{\text{ego}}^{t_r} + v_i^{t_r}$, m_{s_i} is the coefficient regarding the type of O_i ; β is the

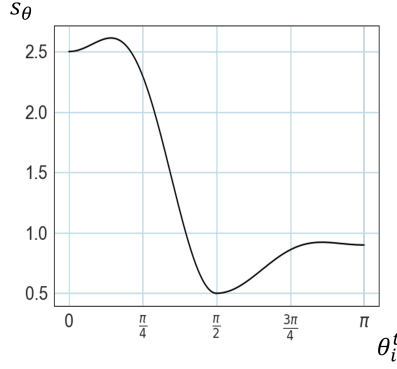


Fig. 3. The relationship between driver's observation sensitivity s_θ and initial angle θ_i^t of traffic object O_i .

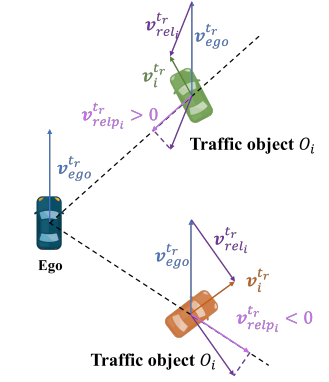


Fig. 4. The calculation methods for $v_{\text{rel}_i}^{t_r}$ and $v_{\text{rel}_i}^{t_r}$.

balancing coefficient of velocity and relative velocity. $v_{\text{rel}_i}^{t_r}$ is the projection of the relative velocity between the ego vehicle and O_i in the direction of their relative position; $v_{\text{rel}_i}^{t_r}$ is the magnitude of the relative velocity vector difference between the ego vehicle and O_i . $v_{\text{rel}_p}^{t_r}$ and $v_{\text{rel}_i}^{t_r}$ are shown in Fig. 4.

On the other hand, if traffic object O_i does not collide with any RPD (the risk perception is not triggered), only the background energy $E_{p_i}^{t_r}$ influenced by the ego vehicle's energy will exist. $E_{p_i}^{t_r}$ is defined in (8).

$$E_{e_i}^t = 1/2m_{s_i}(\beta v_{\text{ego}}^{t_r})^2 \quad (8)$$

III. EXPERIMENT AND DATA COLLECTION

A. Data Preparation

We chose the NuPlan public dataset [17] as the scenario. The dataset includes extensive labeled position and kinematic information of the ego vehicle and surrounding traffic objects, and 360-degree camera view of the ego vehicle. The frequency of the video is 10 Hz. We extracted 113 video clips, with a total duration of 1 hour and 14 minutes. As shown in Fig 5, we extracted the forward, left-front, right-front, and the mirror-rearward views and stitched them together to play on a three-screen simulator. We did not provide other views because they are blind spots for drivers. This can make participants obtain information closely resembles the actual driving process.

B. Experiment Procedure

We recruited 20 participants for SRR collection (5 females and 15 males). All participants hold driving licenses in China. The average driving age of participants is 4.45, and SD is 2.87.

Before the experiment, each driver received an adaptation training to familiarize the rating criteria. During the experiment, real-time SRRs are recorded through the keyboard. The video only plays when the driver holds down a specific rating key, where SRR-1 represents no risk, SRR-2 almost no risk, SRR-3 slight risk, SRR-4 risk, and SRR-5 high risk [13]. We encouraged drivers to provide ratings as quickly as possible based on their intuition. Besides, we asked them to switch ratings quickly to ensure continuous SRRs.

$$s_\theta = \begin{cases} A_\theta (\cos(2\theta_i^t) + 1) + B_\theta (1 - \cos(4\theta_i^t)) + C_\theta, & 0^\circ < \theta < 90^\circ \\ A_\theta (\cos(2\theta_i^t - \pi) + 1) + B_\theta (1 - \cos(4\theta_i^t - \pi)) + C_\theta, & 90^\circ < \theta < 180^\circ \end{cases} \quad (6)$$

$$E_{p_i}^{t_r} = \begin{cases} \frac{1}{2} m_{s_i} \left((1 - \beta) v_{\text{rel}p_i}^{t_r} + \beta v_{b_i}^{t_r} \right) \cdot (\beta (v_{\text{rel}i}^{t_r} + v_{b_i}^{t_r})), & x < 0 \\ \frac{1}{2} m_{s_i} (\beta v_{b_i}^{t_r}) \cdot (\beta (v_{\text{rel}i}^{t_r} + v_{b_i}^{t_r})), & x \geq 0 \end{cases} \quad (7)$$



Fig. 5. Interface for video playback and rating during the experiment. The platform is based on a triple-screen simulator.

TABLE I
ORIGINAL DATA EXTRACTED FROM NUPLAN DATASET

Ego vehicle data		Traffic data	
Parameter name	Symbol	Parameter name	Symbol
Position	x_x, x_y	Position of O_i	x_{x_i}, x_{y_i}
Velocity	v_x, v_y	Velocity of O_i	v_{x_i}, v_{y_i}
Acceleration	a_x, a_y	Acceleration of O_i	a_{x_i}, a_{y_i}
Angle	φ	Angle of O_i	φ_i
-	-	Type of O_i	type_i

C. Data Pre-processing

As shown in Table I, the original data includes the kinematic data of ego vehicle and surrounding traffic objects. For timestamp t , we extract the data of up to 30 closest vehicles and 10 closest pedestrians and input them into DSPR model to obtain the risk matrix $\mathbf{R}(t)$. The size of $\mathbf{R}(t)$ is 1×40 . Road conditions also affect driver's risk perception. We classify them by one-hot encoding: 1-three or fewer lane road, 2-four or more lane road, 3-pavement, 4-controlled intersection, 5-uncontrolled intersection, and 6-mixed-traffic road. The road condition parameter is denoted as C .

The parameters of the ego vehicle, road conditions, and the risk matrix $\mathbf{R}(t)$ are combined to another matrix, denoted as Φ_t and defined in (9). The size of Φ_t is 1×46 . We combine Φ_t of every T timesteps and denote the network input sequences as Ψ_t , as shown in (10). Then, we put Ψ_t into the network.

$$\Phi_t = [v_x \quad v_y \quad a_x \quad a_y \quad \varphi \quad C \quad \mathbf{R}(t)] \quad (9)$$

$$\Psi_t = [\Phi_{t-T+1} \quad \Phi_{t-T+2} \quad \dots \quad \Phi_{t-1} \quad \Phi_t]^T \quad (10)$$

IV. NETWORK TRAINING METHODOLOGY

A. CNN-Bi-LSTM-TPA Network for SRR Prediction

Driver's attention is limited and cannot notice the risk posed by all traffic objects. Besides, it is necessary to consider the time-dependent relationship of risks. Long short-term memory (LSTM) networks can effectively address this

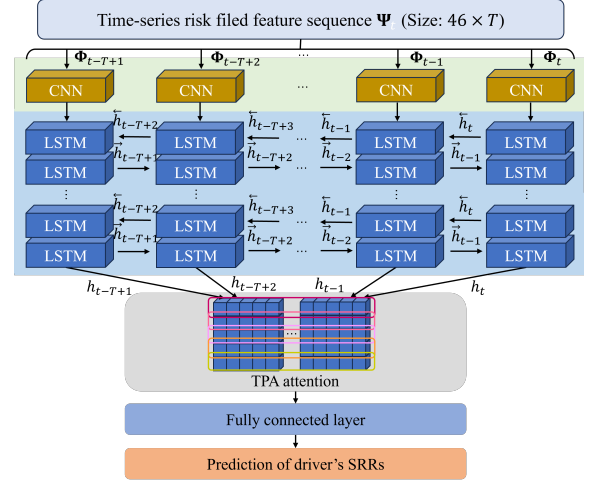


Fig. 6. Structure of CNN-Bi-LSTM-TPA network.

issue [18]. LSTM is widely used in time series processing, and can better capture long-term dependencies in sequences. In our study, we proposed the CNN-Bi-LSTM-TPA network to predict driver's SRRs. The structure is shown in Fig. 6.

1) *CNN layer*. Every CNN receives data from a single time step in Ψ_t . It consists of a convolutional layer, a ReLU activation function layer, and a dropout layer. CNN layer helps the network better understand hidden relationships between features.

2) *Bi-LSTM layer*. The Bi-LSTM layer processes the output of CNN layer. Here, \vec{h}_t and \overleftarrow{h}_t represent the forward and backward hidden states, respectively. After passing through several stacked Bi-LSTM layers, the hidden state h_t of the final layer is output to the attention mechanism.

3) *TPA layer*. We combined the attention mechanisms proposed by Shih et al. [19] The TPA mechanism places greater emphasis on the correlation of features in the temporal domain than traditional attention mechanism.

4) *Fully connected (FC) layer*. The output from the attention layer is processed through an FC layer, which ultimately yields the predicted SRRs.

B. Label Reconstruction and Semi-supervised Learning

Not all SRRs are credible because of driver's subjectivity. To improve the consistency and decrease the noise caused by individual variances of SRRs, we define the consistency ratio p_T^t in (11). Only if p_T^t reaches a certain threshold p_{true} , the rating is marked as a true label.

$$p_T^t = \max \left(\frac{N_r^t}{N} \right) \quad (r = 1, 2, 3, 4) \quad (11)$$

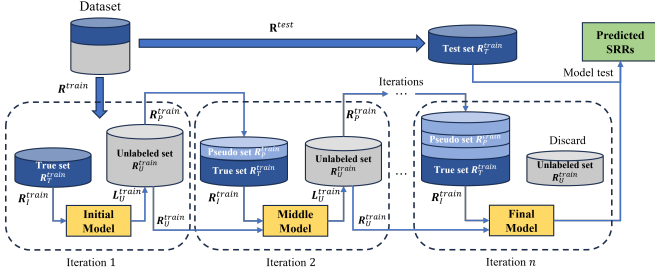


Fig. 7. Semi-supervised learning strategy.

TABLE II
PARAMETERS OF DSPR.

Para	Value	Para	Value	Para	Value	Para	Value
L	4.8	A_θ	1	β	0.12	THW_w	2.4
W	2	B_θ	0.4	$m_{s_i}(v)$	5	THW_s	1.2
t_p	4	C_θ	0.5	$m_{s_i}(p)$	10	-	-

$m_{s_i}(v)$ is m_{s_i} for vehicle. $m_{s_i}(p)$ is m_{s_i} for pedestrian.

where N_r^t is the number of participants of the rating r at t . N is the total number of participants.

According to split ratio s , data are divided into the training set $\mathbf{R}^{\text{train}}$ and the testing set \mathbf{R}^{test} . They are further divided into the true set and the unlabeled set: $\mathbf{R}^{\text{train}} = \{\mathbf{R}_T^{\text{train}}, \mathbf{R}_U^{\text{train}}\}$ and $\mathbf{R}^{\text{test}} = \{\mathbf{R}_T^{\text{test}}, \mathbf{R}_U^{\text{test}}\}$ by (11). At t , if $p_T^t \geq p_{\text{true}}$, it will be included in the true set. Otherwise, included in the unlabeled set. Input sequences and labels are denoted as \mathbf{D} and \mathbf{L} : $\mathbf{R}_T^{\text{train}} = \{\mathbf{D}_T^{\text{train}}, \mathbf{L}_T^{\text{train}}\}$, $\mathbf{R}_T^{\text{test}} = \{\mathbf{D}_T^{\text{test}}, \mathbf{L}_T^{\text{test}}\}$, and $\mathbf{R}_U^{\text{train}} = \{\mathbf{D}_U^{\text{train}}\}$.

Semi-supervised learning are applied for label reconstruction and updating, as shown in Fig. 7 The steps are as follows: 1) Define the input set as $\mathbf{R}_I^{\text{train}} = \{\mathbf{R}_T^{\text{train}}\}$ to train an initial model. 2) Input $\mathbf{D}_U^{\text{train}}$ into the model to generate new label set $\mathbf{L}_U^{\text{train}}$. 3) Labels in $\mathbf{L}_U^{\text{train}}$ with confidence higher than ϵ are selected, denoted as $\mathbf{L}_P^{\text{train}}$. $\mathbf{L}_P^{\text{train}}$ and their corresponding input sequences $\mathbf{D}_P^{\text{train}}$ are added into the pseudo-labeled set $\mathbf{R}_P^{\text{train}} = \{\mathbf{D}_P^{\text{train}}, \mathbf{L}_P^{\text{train}}\}$. Labels with confidence lower than ϵ are returned to $\mathbf{R}_U^{\text{train}}$. 4) Define $\mathbf{R}_I^{\text{train}} = \{\mathbf{R}_T^{\text{train}}, \mathbf{R}_P^{\text{train}}\}$ to train a middle model and repeat step 2) to 4) for several times. 5) After several iterations, discard the rest unlabeled set $\mathbf{R}_U^{\text{train}}$. 6) Define $\mathbf{R}_I^{\text{train}} = \{\mathbf{R}_T^{\text{train}}, \mathbf{R}_P^{\text{train}}\}$ to train a final model. 7) Use $\mathbf{R}_T^{\text{test}}$ to test the final model.

V. RESULTS AND DISCUSSION

A. Parameter

1) *DSPR parameters.* Overall, due to the presence of the LSTM network and the attention mechanism, we don't need to focus too much on the absolute value of DSPR. Instead, the relative risk between different situations is what matters most. DSPR parameters are shown in Table II.

2) *Training parameters.* We set T to 10 (equal to 1 second). split ratio for train set $s = 0.7$. Considering the imbalanced amount of different SRRs, we apply different p_{true} values to each SRR and the SMOTE-NC (Synthetic Minority Over-sampling Technique for Nominal and Continuous) method to augment the minority classes. The p_{true} values and statistics of SRR labels are shown in Table III. Because participants provided significantly fewer ratings

TABLE III

THE p_{true} VALUES AND STATISTICS OF SRRS LABELS.

Dataset	SRR-1	SRR-2	SRR-3	SRR-4*
Total	1403	2013	915	115
p_{true}	0.9	0.75	0.65	0.6
True Label in Train Set	477	35	36	9
True Label in Test Set.	184	17	11	6

*The SRR-5 is merged in SRR-4.

TABLE IV

COMPARISON WITH OTHER RISK ASSESSMENT MODELS.

Model	Precision	Recall	F1-score	AUC
1/TTC	0.5967	0.6522	0.5817	0.8975
DSF	0.7947	0.7880	0.7779	0.9095
PODAR	0.7762	0.7677	0.7501	0.9316
Ours	0.8808	0.8791	0.8789	0.9733

for SRR-4 and SRR-5 (Just 2% among all SRR labels). Distinguishing between SRR-4 and SRR-5 may even result in certain type of SRRs being absent from the training or test sets. Therefore, we merged SRR-4 and SRR-5 into a single level, represented by SRR-4 as indicating risk. After processed by SMOTE-NC, each SRR category is adjusted to the same number of label instances (477 true labels for train set and 184 true labels for test set in each SRR category).

B. The Comparison Study with Other Risk Models

We implement three other different risk assessment methods, the inverse Time to Collision (1/TTC), the Driving Safety Field (DSF) [6], and the Potential Damage Risk (PODAR) [7]. They are calculated for each traffic object and constructed as the same data input structure as DSPR. All models also experienced the same training process in Section IV. Results are shown in Table IV. DSPR shows the best performance in terms of precision, recall, f1 score, and area under the curve (AUC) score among them, presenting advantages in predicting driver's SRRs compared to the other three models.

C. Effectiveness of Semi-supervised Learning Strategy

We compared the results of supervised training with those of semi-supervised training. As shown in Fig. 8, the accuracy of the supervised learning on the original test set \mathbf{R}^{test} is 67.79%. After the label selection and 5 iterations, the accuracy of the semi-supervised learning on true test set $\mathbf{R}_T^{\text{test}}$ is 87.91%, improving the accuracy by 20.12%. Proposed strategy significantly improves the prediction accuracy for SRR-2, SRR-3, and SRR-4. However, there are still some shortcomings in distinguishing between SRR-3 and SRR-4, particularly with SRR-4 often being misclassified as SRR-3. This suggests that there is some disagreement among drivers in SRR-3 and SRR-4, making them difficult to differentiate in certain cases.

D. Comparison studies of Four LSTM Networks

We constructed three different networks (Bi-LSTM, CNN-LSTM, TPA-LSTM) to compare with our network. As shown in Table V, proposed CNN-Bi-LSTM-TPA overall exhibits better performance in precision, recall, f1-score and AUC score. Integrating a CNN network as the preprocessing step

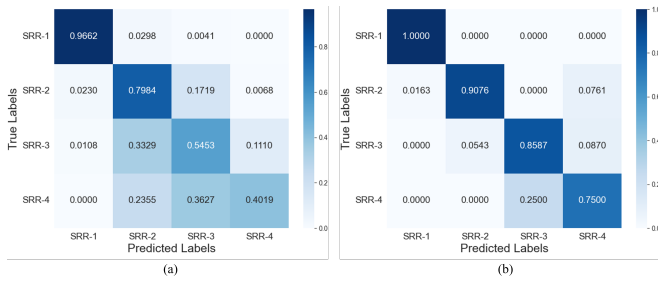


Fig. 8. The confusion matrices of predicted results: (a) Results of supervised learning on R^{est} . (b) Results after label reconstruction and semi-supervised learning strategy on R_T^{est} .

TABLE V

COMPARISON STUDIES OF BI-LSTM, CNN-LSTM, TPA-LSTM AND OUR MODEL

SRRs	Metrics	Model			
		Bi-LSTM	CNN-LSTM	TPA-LSTM	Ours
SRR-1	Precision	1.0000	0.9840	1.0000	0.9840
	Recall	1.0000	1.0000	1.0000	1.0000
	F1-score	1.0000	0.9919	1.0000	1.0000
	AUC	1.0000	1.0000	1.0000	1.0000
SRR-2	Precision	0.5833	0.5825	0.7137	0.9435
	Recall	0.9511	0.9402	0.9348	0.9076
	F1-score	0.7231	0.7193	0.8094	0.9252
	AUC	0.9800	0.9093	0.9857	0.9612
SRR-3	Precision	0.5882	0.6054	0.7600	0.7745
	Recall	0.5435	0.6087	0.8261	0.8587
	F1-score	0.5650	0.6070	0.7917	0.8144
	AUC	0.8687	0.8816	0.9256	0.9766
SRR-4	Precision	0.9512	1.0000	0.9640	0.8214
	Recall	0.4239	0.3641	0.5815	0.7500
	F1-score	0.5865	0.5339	0.7254	0.7841
	AUC	0.9555	0.8038	0.9205	0.9555
Accuracy		0.7296	0.7283	0.8356	0.8791

before the LSTM network allows for more effective extraction of relationships among input features. The attention mechanism further improves the model's ability to capture temporal dependencies. Combining both techniques can lead to enhanced prediction accuracy.

It is evident that all models achieve the best performance for SRR-1, which has a higher consistency. All models find it challenging to distinguish between SRR-3 and SRR-4 due to driver's subjectivity and randomness in rating, which may lead to varied ratings even for similar scenarios.

VI. CONCLUSION

In this paper, we designed a risk-trigger mechanism, spatiotemporal decay, and anisotropy for driver's subjective perceived risk modeling. We conducted a driver-in-the-loop experiment and recruited 20 participants for SRR collection. After selecting high consistency labels among SRRs, we employed a semi-supervised learning strategy with a proposed CNN-Bi-LSTM-TPA network to reconstruct the labels and train the model. Results indicate that our proposed DSPR model presents the highest accuracy in predicting driver's perceived risk compared to the other three risk models. The semi-supervised learning strategy effectively reduces data noise caused by the driver, improving the accuracy by 20.12%. The proposed CNN-Bi-LSTM-TPA network demonstrates the highest accuracy (87.91%) compared to other LSTM network structures.

In future research: (1) We will expand the dataset scenarios and participant pool to study driver's perceived risk more comprehensively; (2) We will develop DSPR model tailored to different driving scenarios to enhance the model's ability; (3) We will explore the relationship between driver's SRRs and DSPR model parameters, with the goal of adaptively optimizing DSPR parameters.

REFERENCES

- [1] S. Wang, Z. Li, Y. Wang, W. Zhao, and T. Liu, "Evidence of automated vehicle safety's influence on people's acceptance of the automated driving technology," *Accid. Anal. Prev.*, vol. 195, p. 107381, 2024.
- [2] Z. Kenesei, K. Asványi, L. Kökény, M. Jászberényi, M. Miskolczi, T. Gyulavári, and J. Syahrivar, "Trust and perceived risk: How different manifestations affect the adoption of autonomous vehicles," *Transp. Res. Part A Policy Pract.*, vol. 164, pp. 379–393, 2022.
- [3] M. Kyriakidis, R. Happee, and J. C. De Winter, "Public opinion on automated driving: Results of an international questionnaire among 5000 respondents," *Transp. Res. Part F Psychol. Behav.*, vol. 32, pp. 127–140, 2015.
- [4] C. Wang, Y. Xie, H. Huang, and P. Liu, "A review of surrogate safety measures and their applications in connected and automated vehicles safety modeling," *Accid. Anal. Prev.*, vol. 157, p. 106157, 2021.
- [5] D. Song, J. Zhao, B. Zhu, J. Han, and S. Jia, "Subjective driving risk prediction based on spatiotemporal distribution features of human driver's cognitive risk," *IEEE Trans. Intell. Transp. Syst.*, 2024.
- [6] J. Wang, J. Wu, and Y. Li, "The driving safety field based on driver-vehicle-road interactions," *IEEE Trans. Intell. Transp. Syst.*, vol. 16, no. 4, pp. 2203–2214, 2015.
- [7] C. Chen, Z. Lan, G. Zhan, Y. Lyu, B. Nie, and S. E. Li, "Quantifying the individual differences of drivers' risk perception via potential damage risk model," *IEEE Trans. Intell. Transp. Syst.*, 2024.
- [8] Z. Xie, Y. Ma, Z. Zhang, and S. Chen, "Real-time driving risk prediction using a self-attention-based bidirectional long short-term memory network based on multi-source data," *Accid. Anal. Prev.*, vol. 204, p. 107647, 2024.
- [9] X. Liu, Y. Zhou, and C. Gou, "Learning from interaction-enhanced scene graph for pedestrian collision risk assessment," *IEEE Trans. Intell. Veh.*, 2023.
- [10] M. R. Endsley, "Toward a theory of situation awareness in dynamic systems," *Hum. Factors*, vol. 37, no. 1, pp. 32–64, 1995.
- [11] X. He, J. Stapel, M. Wang, and R. Happee, "Modelling perceived risk and trust in driving automation reacting to merging and braking vehicles," *Transp. Res. Part F Psychol. Behav.*, vol. 86, pp. 178–195, 2022.
- [12] J. Stapel, A. Gentner, and R. Happee, "On-road trust and perceived risk in level 2 automation," *Transp. Res. Part F Psychol. Behav.*, vol. 89, pp. 355–370, 2022.
- [13] P. Ping, W. Ding, Y. Liu, and K. Takeda, "An enhanced driver's risk perception modeling based on gate recurrent unit network," in *2022 IEEE Intelligent Vehicles Symposium (IV)*. IEEE, 2022, pp. 1234–1240.
- [14] S.-Y. Yu, A. V. Malawade, D. Muthirayan, P. P. Khargonekar, and M. A. Al Faruque, "Scene-graph augmented data-driven risk assessment of autonomous vehicle decisions," *IEEE Trans. Intell. Transp. Syst.*, vol. 23, no. 7, pp. 7941–7951, 2021.
- [15] W. Zhu, X. Zhang, C. Hu, B. Zhao, S. Peng, and H. Yang, "A comfort quantification method based on semi-supervised learning for automated vehicle at lane change scenarios," *IEEE Trans. Intell. Veh.*, vol. 8, no. 5, pp. 3375–3383, 2022.
- [16] H. Hu, Q. Wang, M. Cheng, and Z. Gao, "Cost-sensitive semi-supervised deep learning to assess driving risk by application of naturalistic vehicle trajectories," *Expert Syst. Appl.*, vol. 178, p. 115041, 2021.
- [17] H. Caesar, J. Kabzan, K. S. Tan, W. K. Fong, E. Wolff, A. Lang, L. Fletcher, O. Beijbom, and S. Omari, "Nuplan: A closed-loop ml-based planning benchmark for autonomous vehicles," *arXiv preprint arXiv:2106.11810*, 2021.
- [18] S. Hochreiter, "Long short-term memory," *Neural Comput.*, vol. 9, no. 8, pp. 1735–1780, 1997.
- [19] S.-Y. Shih, F.-K. Sun, and H.-y. Lee, "Temporal pattern attention for multivariate time series forecasting," *Mach. Learn.*, vol. 108, pp. 1421–1441, 2019.